Cell Death and Differentiation (2013) 20, 1404–1414

www.nature.com/cdd

Granzyme B degrades extracellular matrix and contributes to delayed wound closure in apolipoprotein E knockout mice

PR Hiebert[1,2], D Wu[1] and DJ Granville*[,1,2]

Chronic inflammation and excessive protease activity have a major role in the persistence of non-healing wounds. Granzyme B (GzmB) is a serine protease expressed during chronic inflammation that, in conjunction with perforin, has a well-established role in initiating apoptotic cell death. GzmB is also capable of acting extracellularly, independent of perforin and can degrade several extracellular matrix (ECM) proteins that are critical during wound healing. We used apolipoprotein E (ApoE) knockout (AKO) mice as a novel model of chronic inflammation and impaired wound healing to investigate the role of GzmB in chronic wounds. Wild-type and AKO mice were grown to 7 weeks (young) or 37 weeks (old) of age on a regular chow or high-fat diet (HFD), given a 1-cm diameter full thickness wound on their mid dorsum and allowed to heal for 16 days. Old AKO mice fed a HFD exhibited reduced wound closure, delayed contraction, chronic inflammation and altered ECM remodeling. Conversely, GzmB/ApoE double knockout mice displayed improved wound closure and contraction rates. In addition, murine GzmB was found to degrade both fibronectin and vitronectin derived from healthy mouse granulation tissue. In addition, GzmB-mediated degradation of fibronectin generated a fragment similar in size to that observed in non-healing mouse wounds. These results provide the first direct evidence that GzmB contributes to chronic wound healing in part through degradation of ECM.
Cell Death and Differentiation (2013) **20**, 1404–1414; doi:10.1038/cdd.2013.96; published online 2 August 2013

Chronic wounds are a growing problem in the developed world due to increasing incidence of diabetes, obesity and aging.[1] Estimates suggest approximately 6 million people suffer from chronic wounds in the United States alone with billions of dollars spent on treatment every year.[1,2] Numerous treatment strategies have been tested in the search for improved therapies. However, chronic wounds remain a major problem. This is partly due to the complex nature of wound healing, which requires a precisely orchestrated immune response and numerous cell–cell/cell–matrix interactions. In a chronic wound, persistent inflammation contributes to excessive proteolysis, which presents a major obstacle in the path toward proper healing and remodeling of wounded tissue.

Granzyme B (GzmB) is a serine protease that is expressed by several types of immune cells during chronic inflammation.[3] GzmB is a known inducer of apoptosis, often used by natural killer (NK) cells and CD8+ T cells to kill virally infected and/or tumor cells by cleaving substrates inside the cytoplasm of the target cell in a process also requiring the membrane disrupting protein perforin.[4–6] Emerging evidence is also confirming the decades old suspicion that GzmB may possess additional non-cytotoxic, perforin-independent roles such as extracellular matrix (ECM) proteolysis and cytokine processing.[3,7,8] These developments have led to a renewed interest in the expanding role of GzmB in health and disease.[3,9] Several lines of evidence also suggest that GzmB-mediated proteolysis may contribute to chronic wound healing.[10]

Apolipoprotein E (ApoE) is a glycoprotein that has a critical role in lipid transport. ApoE knockout (AKO) mice lack the ability to effectively clear circulating cholesterol and become hyperlipidemic.[11,12] ApoE is expressed in multiple tissues including the skin and can also exert important immunosuppressive roles that extend beyond its role in lipid trafficking.[13–16] AKO mice are therefore susceptible to chronic inflammatory skin diseases that often increase in severity to the point where euthanasia is required.[17,18] In addition, aged AKO mice fed with a high-fat diet (HFD) exhibit skin thinning and a loss of dermal collagen density, both common features in elderly individuals who struggle with skin tearing and impaired/chronic wound healing.[17] The effect of age, diet and proper nutrition on healthy aging and wound healing is well documented and known to elicit profound influences over the speed and quality of cutaneous wound repair.[19,20] Diet and/or age-related immune dysfunction could also conceivably give rise to increased levels of GzmB, especially during chronic inflammation.

Previously, we have demonstrated that GzmB contributes to accelerated skin aging in HFD-fed AKO mice, featuring skin

[1]UBC James Hogg Research Centre, St. Paul's Hospital, University of British Columbia, Vancouver, British Columbia, Canada and [2]Department of Pathology and Laboratory Medicine, University of British Columbia, Vancouver, British Columbia, Canada
*Corresponding author: DJ Granville, UBC James Hogg Research Centre, St. Paul's Hospital, University of British Columbia, 166-1081 Burrard Street, Vancouver, British Columbia, Canada V6Z 1Y6. Tel: +604 806 9267; Fax: +604 806 9274; E-mail: david.granville@hli.ubc.ca
Keywords: Granzyme B; extracellular matrix; wound healing; skin; inflammation
Abbreviations: ApoE, apolipoprotein E; AKO, apolipoprotein E knockout; ECM, extracellular matrix; GzmB, granzyme B; DKO, granzyme B/ApoE double knockout; HFD, high-fat diet; H&E, hematoxylin and eosin; NK, natural killer; WT, wild type
Received 17.3.13; revised 03.5.13; accepted 06.6.13; Edited by C Borner; published online 02.8.13

thinning and collagen disorganization.[17] GzmB-mediated degradation of the ECM, specifically the proteoglycan decorin, was found to be a likely contributor to the loss of collagen organization observed with age in these mice. In the present study, we explored the use of aged, HFD-fed AKO mice as a model that mimics chronic inflammation and impaired wound healing. As GzmB has been shown to influence skin aging and ECM remodeling in these mice, we also examined the role of GzmB during wound healing in HFD-fed AKO mice.

Results

Impaired wound healing in HFD-fed AKO mice. To determine the influence of age and diet on wound healing in AKO mice, both wild-type (WT) and AKO mice were wounded at 7 (young) or 37 (old) weeks of age. Old mice were fed either a high-fat or regular chow diet beginning at 7 weeks of age. When fed a HFD for 30 weeks, AKO mice exhibited delayed wound healing compared with WT mice (Figure 1a). After healing for 16 days, only 40% of the HFD-fed AKO mice were able to achieve full wound closure compared with 100% of WT mice (Figures 1b and c). In contrast, both WT and AKO mice fed a regular chow diet all showed full wound closure by day 16 regardless of age (Supplementary Figure 1). To determine if GzmB contributes to the delayed wound healing observed in the HFD-fed AKO mice, old ApoE/GzmB double knockout (DKO) mice fed a HFD were also examined. GzmB deficiency resulted in improved wound healing with the majority (80%) of DKO mice achieving full wound closure by day 16 (Figures 1a–c). These results suggest that GzmB contributes to delayed wound healing in HFD-fed AKO mice.

During healthy wound healing, following fusion of the migrating keratinocyte layers, epidermal hyperproliferation decreases and epidermal thickness eventually returns to normal. In the young WT mice, epidermal thickness at day 16 averaged approximately 24 μm (Figure 1d). Epidermal thickness appeared to be greater when older mice were examined at day 16 and was significantly thicker in wounds from the few HFD-fed AKO mice that managed to close (Figure 1d). DKO mice fed a HFD appeared to have reduced epidermal thickness on average compared with the HFD-fed AKO mice at day 16, although this difference failed to reach significance (Figure 1d). These results support the above observation that wound healing is impaired in HFD-fed AKO mice and that even in situations when wound closure is achieved, proper tissue remodeling is significantly delayed.

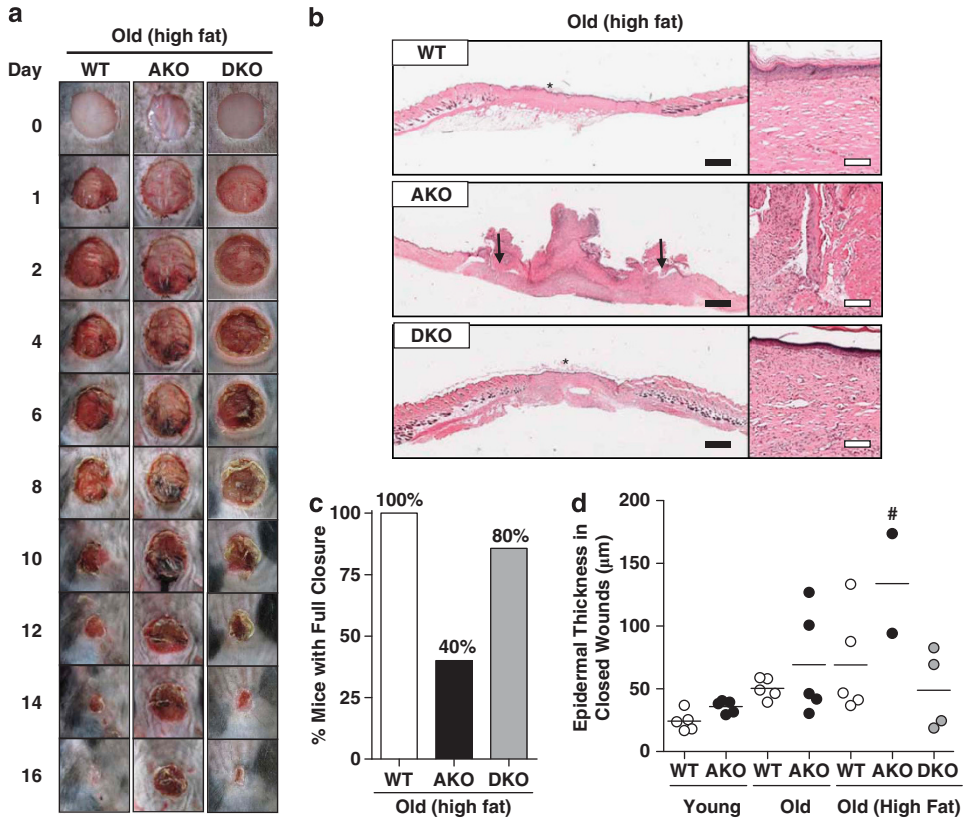

Figure 1 GzmB deficiency improves wound closure in HFD-fed AKO mice. (**a**) Representative images and (**b**) histological cross-sections of wounds from WT ($n=5$), AKO ($n=5$) and DKO ($n=5$) mice over the 16-day healing period. Arrows indicate keratinocyte edges. Asterisks indicate a closed wound. (**c**) All of the WT mice (5/5) showed complete wound closure at day 16, compared with only 40% (2/5) of the AKO mice. GzmB deficiency improved this outcome with 80% (4/5) achieving full wound closure. (**d**) Of the wounds that closed, epidermal thickness was significantly greater in the HFD-fed AKO mice compared with the young WT controls. $^{\#}P<0.05$ *versus* WT (Young); Kruskal–Wallis test with Dunn's multiple comparison post test. Black scale bars = 1 mm, white scale bars = 100 μm

Weight loss. When pre-operation weights were examined, AKO mice fed a HFD weighed significantly less than HFD-fed WT control mice (Figure 2a), confirming results reported previously.[17] Interestingly, GzmB deficiency prevented this weight loss, with the HFD-fed DKO mice on average weighing significantly more than the AKO mice, similar to the WT group (Figure 2a). As anticipated, when weight was monitored over the 16-day healing period, the obese WT mice fed a HFD showed clear weight loss following surgery (Figure 2b). This weight loss was also observed in the DKO mice, although slightly less (Figure 2b). AKO mice, although weighing less to begin with, showed relatively little weight loss ($\sim$7%) during the healing period when compared with the WT mice.

Wound contraction. Contraction has an important role in cutaneous wound healing and was measured in all groups following surgery. In every case, wound sizes initially expanded before contraction. Wounds from the young WT and AKO mice healed primarily by contraction, accounting for approximately 86% of wound closure (Figure 3a). Following the initial expansion period, young WT wounds contracted back to 0% by day 4, while AKO mice took closer to 6 days to contract back to 0% (Figure 3a). Overall, however, contraction rates were similar for both young WT and AKO mice with no significant differences observed.

The effect of age on wound contraction was clearly noticeable when old WT and AKO mice were examined (Figure 3a). Contraction rates again were similar between genotypes, however, when compared with the young mice, the old mice showed a significantly slower contraction rate (Figure 3a), suggesting that age delays wound contraction and closure in both WT and AKO mice. Although the initial rate of expansion immediately following wounding was similar between young and old mice, it took longer for the wounds to contract back to 0% (about 9 days) compared with the young mice who contracted back to 0 by 4 (WT) and 6 (AKO) days. At day 16, the final percent of wound closure achieved by contraction was less in the old mice (74%) compared with the young mice that healed approximately 86% by contraction (Figure 3a).

The influence of diet on wound contraction was also examined (Figure 3b). A HFD failed to induce a significant delay in wound contraction in WT mice when compared with WT mice fed a regular chow diet (Figure 3b). However, when AKO mice were fed a HFD, wound contraction was significantly slower compared with the HFD-fed WT mice and the regular chow-fed mice (Figure 3b). The initial expansion of wound size in HFD-fed AKO mice did not contract back to 0% until day 12, compared with 7–9 days for the other old groups (Figure 3b). These results suggest that delayed contraction is a main contributor to impaired wound healing observed in HFD-fed AKO mice.

To determine whether GzmB deficiency improves wound healing in AKO mice through faster contraction, contraction rates in HFD-fed DKO mice were also examined. As shown in Figure 3c, there was a significant difference in the contraction curve of the DKO mice compared with the AKO mice, with the DKO group demonstrating a consistent increase in the percent of contraction throughout the 16-day period. This included reduced expansion of the wound immediately following wounding, and faster contraction back to 0% and improved wound closure. Interestingly, no significant difference in α-smooth muscle actin staining was observed between the HFD-fed WT, AKO and DKO groups, suggesting altered wound contraction in these mice is not due to differing levels of myofibroblasts (Figure 3d).

Re-epithelialization. To determine whether re-epithelialization was also affected in AKO mice, histological cross-sections were examined at 2, 8 and 16 days post-wounding and re-epithelialization distance was measured (Figure 4). Re-epithelialization was evident in all groups as early as 2 days and became more advanced by day 8 (Figure 4). At day 16, closed wounds in young mice exhibited less re-epithelialization compared with the old groups, likely due to faster contraction leading to quicker wound closure and a reduced need for re-epithelialization (Figure 4). At 2 and 8 days, the amount of re-epithelialization was similar between genotypes fed a HFD, confirming that the delayed wound closure in the HFD-fed AKO model, as well as the improved closure in DKO mice, is primarily due to

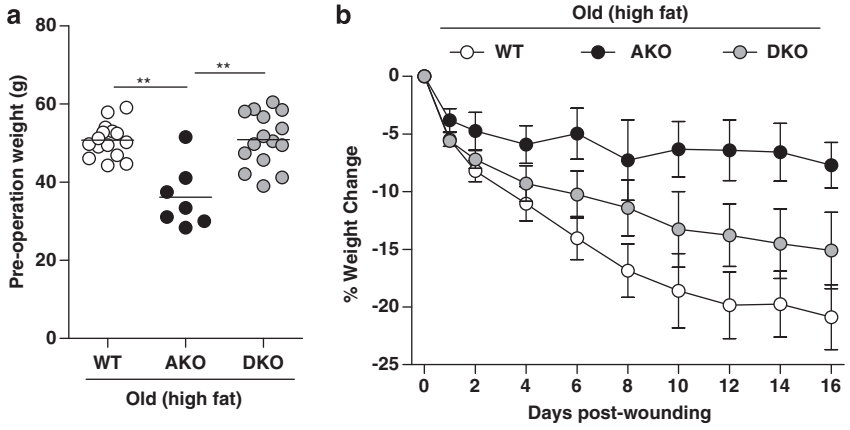

Figure 2 Animal weights before and during wounding. (**a**) Pre-operation weights and (**b**) percent weight change following wounding in WT, AKO and DKO mice fed a HFD for 30 weeks. $^{**}P < 0.01$; Kruskal–Wallis test with Dunn's multiple comparison post test

differences in contraction rather than re-epithelialization (Figure 4).

Inflammation. Several reports have documented the suppressive effects of ApoE on inflammation.[13–16] We therefore examined wounded skin tissue from mice fed a HFD at day 16, to determine whether unresolved inflammation was present in the wounds of HFD-fed AKO mice. At day 16, the wounded skin of HFD-fed AKO mice contained considerable numbers of immune cells including neutrophils, macrophages, T cells and lipid-loaded foam cells (Figure 5a). Compared with the acute wounds in young WT mice, there were significantly more neutrophils in the wounded tissue of HFD-fed AKO mice (Figure 5b). The numbers of macrophages and T cells appeared to vary somewhat within the individual groups and no significant differences were detected regardless of age, diet or genotype (Figures 5c and d). HFD-fed AKO mice also exhibited a significant increase in the numbers of foam cells compared with the young WT mice (Figure 5e). Significant elevations in foam cell numbers were also observed in regular diet-fed AKO mice and HFD-fed DKO mice at day 16 (Figure 5e).

Collagen and decorin levels in wounded skin. GzmB-mediated decorin degradation was found to be a potential mechanism behind collagen disorganization and accelerated

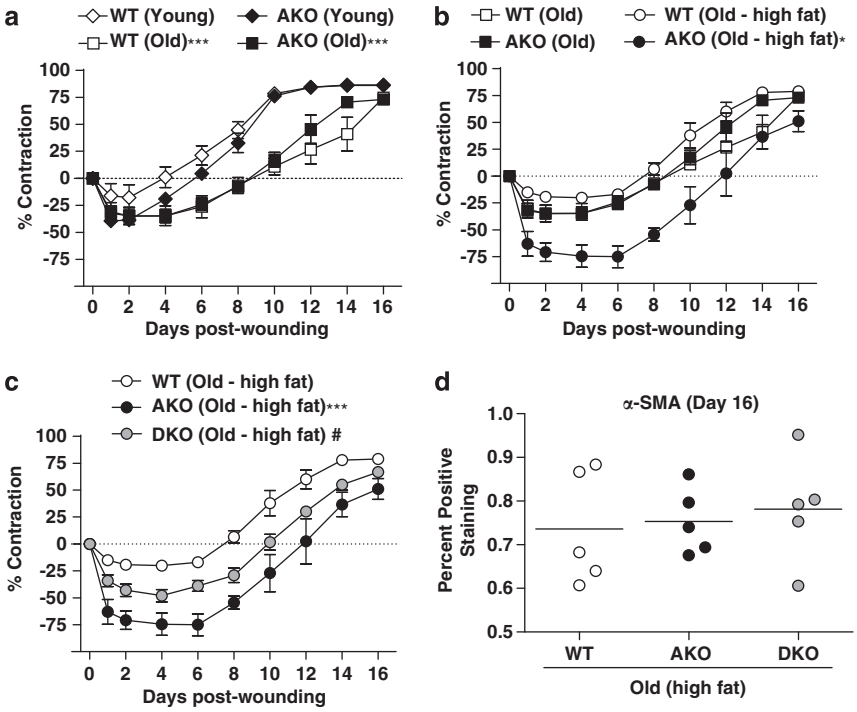

Figure 3 Wound contraction. (**a**) Delayed contraction was observed when mice were aged 30 weeks in both the WT and AKO groups; ***$P<0.005$ *versus* WT (young) and AKO (young). (**b**) A HFD resulted in delayed wound contraction only in the AKO mice; *$P<0.05$ *versus* WT (old), WT (old—high fat) and AKO (old). (**c**) GzmB deficiency improves wound contraction in HFD-fed AKO mice; ***$P<0.005$ *versus* WT (old – high fat), #$P<0.01$ *versus* AKO (old – high fat). (**d**) No significant differences in α-SMA staining were observed between genotypes when fed a HFD. *P*-values were calculated using two-way repeated measures ANOVA (**a**–**c**) and Kruskal–Wallis test with Dunn's multiple comparison post test (**d**)

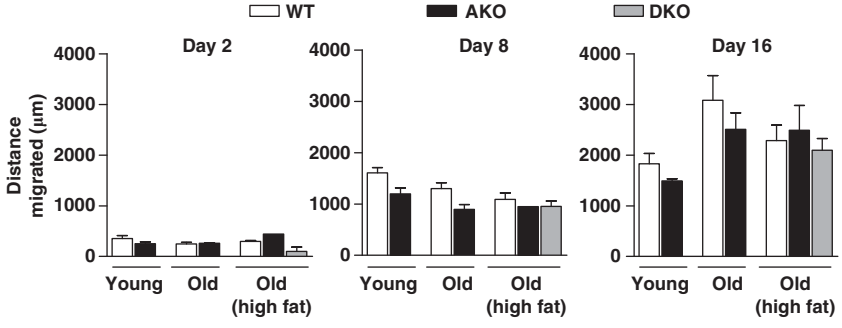

Figure 4 Re-epithelialization distances. Re-epithelialization distance was measured at 2, 8 and 16 days post-wounding. No significant differences in re-epithelialization were observed regardless of age, diet or genotype. Error bars represent ± S.E.M. (Kruskal–Wallis test with Dunn's multiple comparison post test)

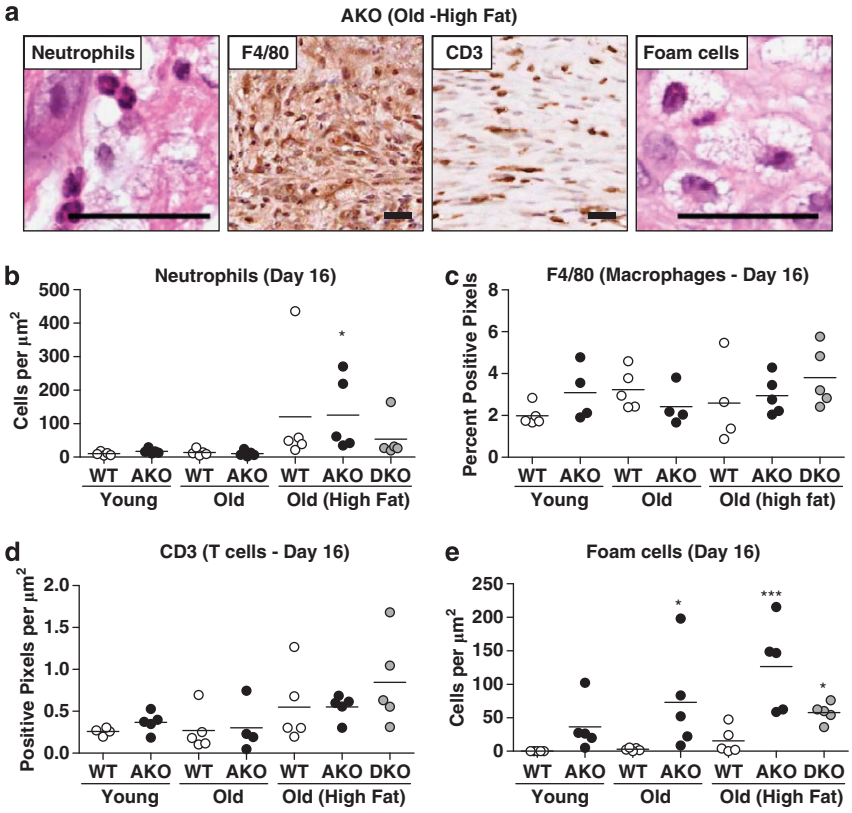

Figure 5 Persistent inflammation in HFD-fed AKO mouse wounds. (**a**) Granulation tissue at day 16 from HFD-fed AKO mice contained numerous inflammatory cells including neutrophils, macrophages (F4/80), T cells (CD3) and foam cells. HFD-fed AKO mice contained significantly more neutrophils (**b**) at day 16 compared with the young WT controls. No significant differences were observed in F4/80 and CD3-stained sections (**c** and **d**). Old AKO mice fed a chow or a HFD demonstrated significantly more foam cells, as did HFD-fed DKO mice when compared with young WT controls (**e**). $^{*}P<0.05$, $^{***}P<0.005$ *versus* young WT mice. *P*-values were calculated using Kruskal–Wallis test with Dunn's multiple comparison post test. Scale bars = 25 μm

skin aging in HFD-fed AKO mice.[17] To examine the status of decorin in HFD-fed AKO mice undergoing wound healing, we performed immunohistochemistry analysis for decorin at day 16 in wounded skin cross-sections from mice with closed wounds. Young WT mice showed decorin staining throughout the newly formed dermis with the most intense staining seen near the dermal–epidermal junction (Figure 6a). Decorin levels were similar in the young AKO mice but appeared to be reduced in the old mice although this difference failed to reach significance (Figure 6b). Decorin levels were low in the closed wounds of the HFD-fed AKO mice, whereas several DKO mice appeared to have considerably more intense decorin staining by comparison (Figures 6a and b).

Collagen content in the wounded skin tissue at day 16 was also examined using picrosirius red. Similar to what was observed with decorin, the greatest amount of collagen observed was in the young WT mice (Figures 6a and c). Both the HFD-fed WT and AKO mice (but not the DKO mice) demonstrated significantly less collagen staining in the closed wounds compared with the young WT controls (Figure 6c).

Fibronectin and vitronectin levels during wound healing. The glycoproteins fibronectin and vitronectin both have important roles to play in normal wound closure and remodeling.[21] The granulation tissue contains a provisional matrix rich in fibronectin and vitronectin, which helps to mediate wound contraction through various interactions with collagen, other matrix proteins and several integrins found on contractile cells.[22–26] To determine the status of fibronectin and vitronectin in our wound-healing model, skin sections from young WT mice were harvested at the wounded site, homogenized and analyzed for these ECM components by western blot. Both fibronectin and vitronectin levels in wounded skin increased at days 2 and 8 post-wounding when compared with the original, unwounded skin (Figure 7a). Levels of fibronectin and vitronectin were greatest at day 8, corresponding to the increased deposition of granulation tissue. By day 16, fibronectin and vitronectin levels again resembled the original, unwounded skin, representing near complete tissue remodeling and replacement of the provisional matrix with collagen (Figure 7a).

Mouse GzmB degrades fibronectin and vitronectin in granulation tissue. Although GzmB cleavage of fibronectin and vitronectin has been confirmed in multiple studies,[27–29] these experiments have focused only on the activity of human GzmB on human ECM proteins. As mouse and human GzmB are known to differ in terms of their effectiveness at cleaving certain intracellular substrates,[30]

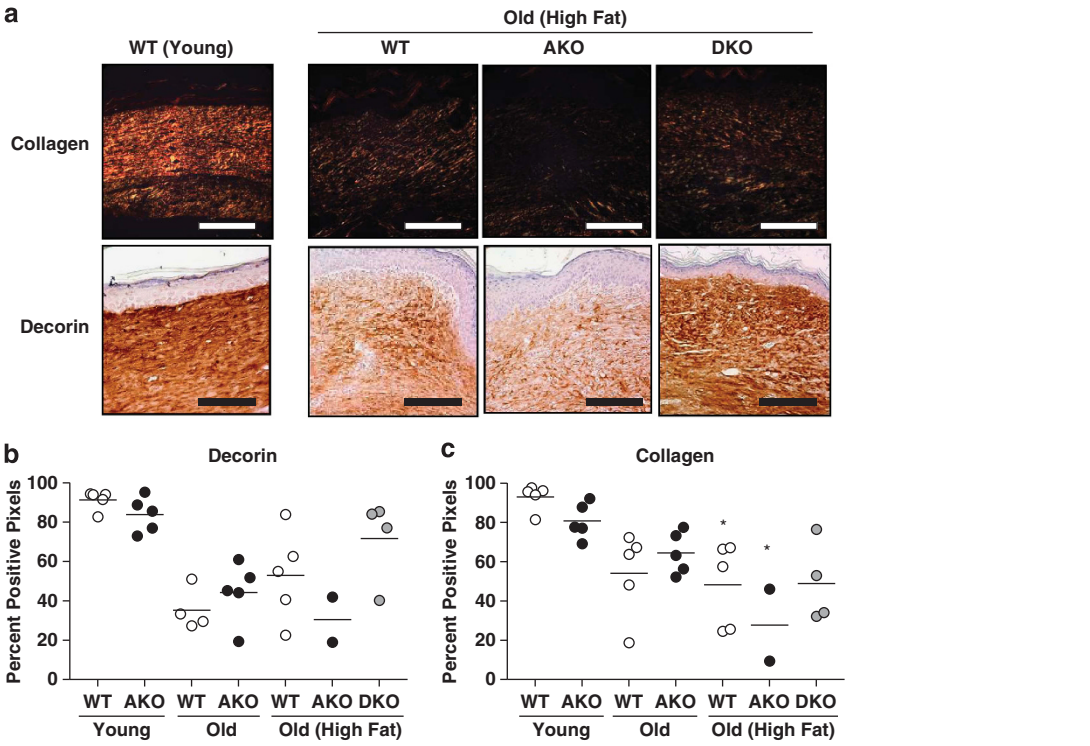

Figure 6 Collagen and decorin content in closed wounds at day 16. (**a**) Representative images of HFD-fed wounded mouse skin cross-sections at day 16 compared with young WT mice stained with either picrosirius red or decorin. (**b**) Decorin and (**c**) collagen quantification within the granulation tissue of all groups of mice. Both WT and AKO mice fed a HFD exhibited significantly reduced collagen levels compared with the young WT controls. *$P<0.05$ *versus* young WT mice, Kruskal–Wallis test with Dunn's multiple comparison post test. Scale bars = 200 μm

we tested the ability of recombinant mouse GzmB to degrade both mouse fibronectin and vitronectin derived from the granulation tissue of wounded mice. Mouse GzmB was incubated with the homogenized skin tissue from wounded WT mice at day 8 and analyzed for fibronectin/vitronectin fragmentation by western blot (Figure 7b). Day 8 was chosen as it had the highest amount of these ECM proteins (Figure 7a). As shown in Figure 7b, mouse GzmB cleaved granulation tissue-derived fibronectin and vitronectin at as low as 100 nM in a dose-dependent manner. Increasing concentrations of GzmB resulted in the complete degradation of the full-length fibronectin band at ~250 kDa, while increasing the presence of a lower–molecular-weight band at ~220 kDa (Figure 7b). Similarly, increasing concentrations of GzmB degraded the full-length vitronectin band at 75 kDa, eventually leaving only the 65-kDa fragment, which also appeared to be reduced compared with when no GzmB was added.

To investigate the *in vivo* effect of GzmB on the proper functioning and remodeling of these ECM components in our chronic wound model, skin from HFD-fed WT, AKO and DKO mice was analyzed for fibronectin and vitronectin by western blot (Figure 7c). All WT mice examined at day 16 showed relatively little fibronectin levels similar to the young WT controls (Figures 7a and c). Similar observations were made for vitronectin when WT mice were examined at day 16. AKO mice on the other hand showed increased fibronectin and vitronectin content at day 16 including significantly increased amounts of a fibronectin fragment measuring ~220 kDa, similar in size as the fragment generated by GzmB (Figures 7b–d). The majority of DKO mice on the other hand, with one exception, showed fibronectin and vitronectin levels similar to the WT group, suggesting similar ECM remodeling took place during wound healing as in WT mice. Interestingly, a ~220-kDa fibronectin fragment was also observed in the one outlier DKO mouse (Figure 7c), suggesting that other proteases in addition to GzmB are also capable of generating a ~220-kDa fibronectin fragment. When immunohistochemistry for GzmB in the non-healed skin of HFD-fed AKO mice was examined, GzmB-positive staining was observed throughout the granulation tissue of the non-healed wounds (Figure 7e). Taken together, these results suggest that GzmB is present locally at the site of injury and contributes to impaired wound healing in HFD-fed AKO mice, possibly through direct remodeling of ECM proteins such as fibronectin and vitronectin.

Discussion

GzmB is a multi-functional serine protease with many diverse roles in health and disease.[3,7,8] In addition to its well-established role in cell death, GzmB is also capable of degrading the ECM with the list of identified substrates continuing to increase.[27,28,31–33] GzmB can also regulate inflammation by cleaving and activating cytokines such as IL-18 and IL-1α.[34,35] Interestingly, it is also known that GzmB-mediated cleavage of IL-1α can occur extracellularly by GzmB derived from NK cells,[35] further highlighting the

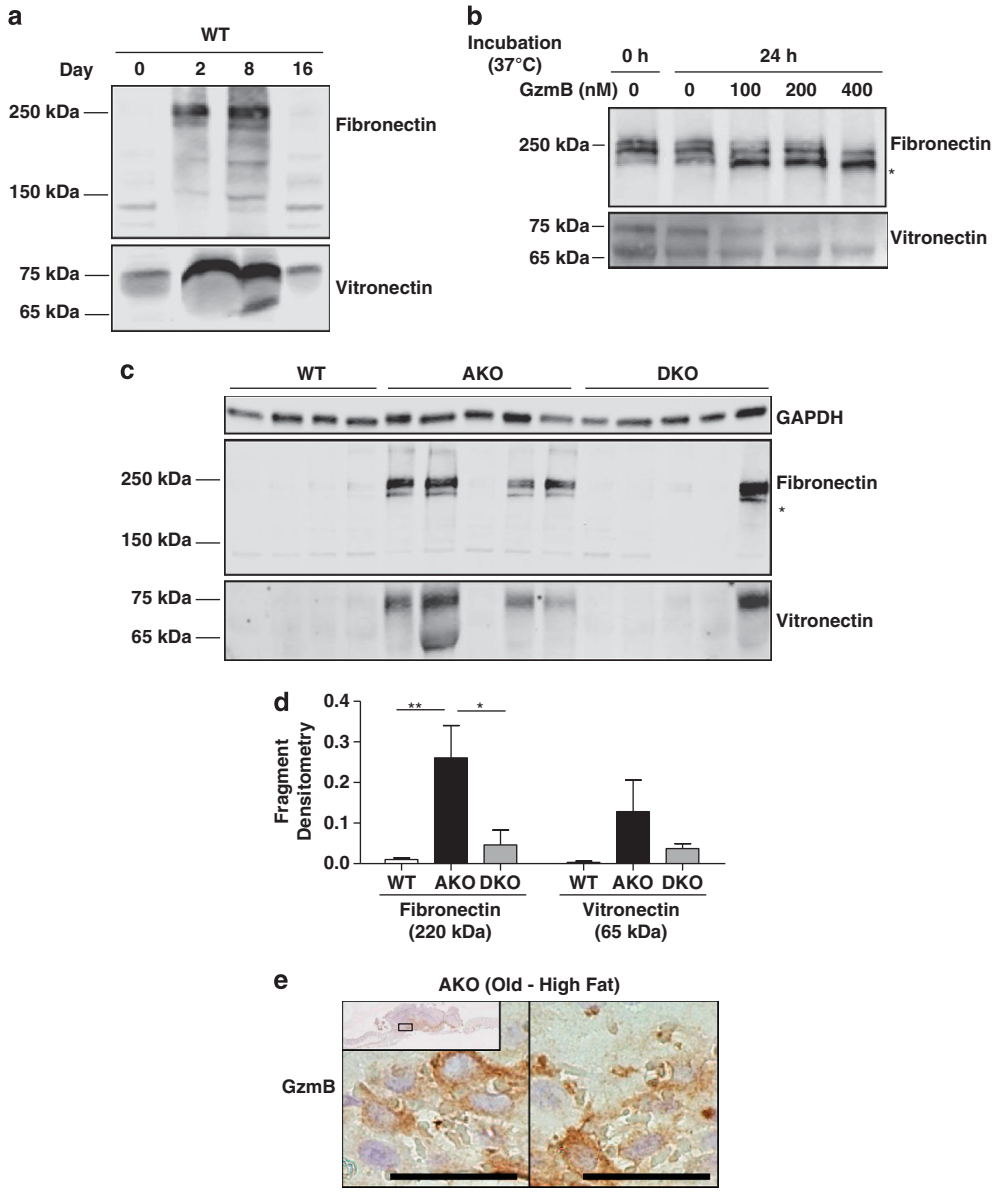

Figure 7 Fibronectin and vitronectin content during wound healing. (**a**) Wounded skin from WT mice was analyzed at days 0, 2, 8 and 16 for fibronectin and vitronectin by western blot. Before wounding (day 0), both fibronectin and vitronectin content is relatively low. Beginning from day 2 to day 8, granulation tissue forms, featuring an increase in fibronectin and vitronectin that returns to normal on day 16. (**b**) Mouse GzmB was added to the skin homogenate from a WT mouse harvested at day 8 post-wounding. As little as 100 nM of GzmB was sufficient to degrade the full-length fibronectin and vitronectin proteins and generate a fibronectin fragment at ~220 kDa. (**c**) AKO mice exhibited increased fibronectin and vitronectin content including the ~220 kDa fibronectin fragment, which appeared to be reduced but not eliminated by knocking out GzmB. (**d**) The 220-kDa fibronectin fragment and the 65-kDa vitronectin fragment were quantified by densitometry. (**e**) GzmB staining was evident within the granulation tissue of HFD-fed AKO mice at day 16. Both images taken from the same wound (inset shows the low magnification image). $^{*}P<0.05$ and $^{**}P<0.01$, two-way ANOVA with Bonferonni post test. Scale bars = 25 μm

potential importance of perforin-independent GzmB activity in health and disease. In fact, both cytotoxic and non-cytotoxic activities of GzmB are suggested to have a role in many inflammatory disorders such as diabetes, cancer, transplant rejection, autoimmunity, cardiovascular and pulmonary diseases (reviewed in refs [36–40]). Although its role in wound healing has never been assessed, considerable evidence exists that would support a role for GzmB in chronic wounds.[10] Immune cell types present in chronic wounds, such as T lymphocytes and macrophages, express GzmB during chronic inflammation,[3,41,42] whereas several GzmB substrates including fibronectin and decorin are well known to have critical roles to play in healthy wound healing.[10,21,43] To our knowledge, this is the first study to directly implicate GzmB in the pathogenesis of chronic wound healing.

In this study, we describe a novel mouse model of chronic wound healing. Aged AKO mice fed a HFD demonstrated reduced contraction, impaired wound closure and persistent inflammation featuring neutrophils, macrophages and lymphocytes. Among the few HFD-fed AKO wounds that did heal by day 16, reduced collagen and increased epidermal thickness were observed compared with WT controls,

suggesting that wound healing and proper tissue remodeling were delayed in closed wounds as well. We also found evidence that GzmB contributed to chronic wound healing and delayed contraction in AKO mice, possibly through the degradation of ECM components such as fibronectin and/or decorin. To our knowledge, this is the first study to directly implicate GzmB in the pathogenesis of chronic wound healing.

Both age and diet were necessary for inducing impaired healing in AKO mice. As shown in this study, the negative effects of age and diet on wound repair were reduced by preventing GzmB activity. These data are in line with previous work demonstrating a role for GzmB in age and diet-induced skin aging.[17] Both age and diet are known to have important impacts on the immune system[44–46] and although there remains much work to be done in uncovering the specific links between aging, diet and GzmB, these data support the notion that age and diet can influence immune dysfunction resulting in elevated levels of GzmB.

ApoE is known to function in a number of roles in the body besides lipid transport. Among those are its ability to influence inflammation.[13–16] Specifically, ApoE has been shown to suppress neutrophil and macrophage activation as well as lymphocyte proliferation. AKO mice fed a HFD for 30 weeks contained increased numbers of neutrophils in the wounded tissue compared with the young WT mice, suggesting localized inflammation in the wounds of HFD-fed AKO mice is persistent and slower to resolve, similar to chronic wounds in humans that also feature persistent neutrophil infiltration.[47] Interestingly, no significant differences were detected in the amount of CD3 or F4/80-positive staining in any of the groups at day 16. It is unknown if T cells or macrophages in AKO mouse wounds have differences in activation profiles compared with the WT controls but this remains a possibility. In addition, macrophage foam cells were observed in the wounded tissue of AKO mice on day 16, reflecting the high-lipid content and are typical cell types present in diseased AKO mouse skin.[17,18] Taken together, HFD-fed AKO wounds demonstrate important signs of persistent inflammation commonly seen in chronic wounds and implicate the HFD-fed AKO mouse as a potentially useful tool to study chronic wound healing.

Decorin is a small leucine-rich proteoglycan that binds to collagen and facilitates proper collagen organization, spacing and tensile strength in the skin.[48,49] In the present study, closed wounds from DKO mice exhibited intense decorin staining compared with closed wounds from AKO mice. These data support previous observations made in the skin of aged AKO mice fed a HFD.[17] This increased decorin was also associated with significantly greater collagen density and organization in DKO mice compared with AKO mice. Decorin knockout mice possess highly disorganized collagen and increased skin fragility that is prone to tearing and have impaired wound healing.[43,48] Excessive degradation of decorin by GzmB during wound healing could negatively impact collagen deposition and remodeling. Interestingly, GzmB-mediated decorin degradation also contributes to blood vessel destabilization and rupture in a model of abdominal aortic aneurysm.[50] The results of the present study provide further evidence for a role for GzmB in impaired tissue repair and prolonged healing in a skin model of chronic wound healing.

Physiologic wound healing requires considerable ECM remodeling and the eventual replacement of the provisional matrix with new collagen fibers. Although proteases and remodeling events are crucial for proper healing, augmented or dysregulated proteolysis can result in excessive degradation of key ECM proteins leading to impaired wound healing.[51,52] For example, increased fibronectin mRNA levels are found in fibroblasts isolated from chronic wounds, whereas reduced full-length fibronectin, along with increased fibronectin and vitronectin fragmentation, is seen in chronic wound fluid compared with acute wound fluid, suggesting excessive ECM proteolysis occurs in chronic wounds.[51–54] In the present study, increased fibronectin and vitronectin levels were observed in wounded tissue of AKO mice at day 16 compared with WT mice with increased fragments. We also found that, similar to human GzmB, murine GzmB is also capable of cleaving fibronectin and vitronectin derived from the granulation tissue of mouse wounds. Fibronectin is an abundant glycoprotein during wound healing and a major component of the provisional matrix that forms during clotting and granulation tissue formation. Fibronectin can act as a temporary physical scaffold while binding/presenting growth factors important for cell proliferation and wound repair. In addition, fibronectin and vitronectin can both bind to a number of integrins on cells.[55] Of interest, vitronectin and fibronectin–integrin interactions influence contraction.[22,24–26] Fibronectin proteolysis by chymotrypsin and cathepsins B and D exposes integrin-binding sites such as the RGD (Arg-Gly-Asp) site thereby enhancing integrin binding.[24,56] It is currently unknown where exactly GzmB cleaves fibronectin, however, GzmB preferentially cleaves after Asp residues[57,58] and Buzza *et al.* have demonstrated that GzmB cleaves vitronectin at the RGD integrin-binding site.[27] Although fibronectin proteolysis by some proteases can enhance integrin binding and contraction,[24,56] GzmB-mediated proteolysis may have profoundly different effects depending on the site of cleavage and, although not confirmed, could negatively influence contraction should integrin binding to the RGD site be disrupted. In our study, we demonstrate that HFD-fed AKO mice express GzmB within the granulation tissue, contain elevated levels of a fibronectin fragment similar to that generated by GzmB *in vitro,* which corresponds with significantly delayed wound contraction that was improved in DKO mice. Future work is needed to further characterize the exact role of GzmB-mediated degradation of fibronectin and vitronectin in this model and its effect on contraction.

In summary, AKO mice fed a HFD exhibit impaired wound healing. We also provide the first direct evidence that GzmB contributes to chronic wound healing through the degradation of ECM proteins. Future studies investigating the AKO mouse in wound healing and the role of GzmB in chronic wounds are sure to uncover additional insights into the mechanisms involved in the persistence of chronic wounds.

Materials and Methods

Animals and diets. Animal procedures described were performed in accordance with the appropriate University of British Columbia (UBC) guidelines for animal experimentation and approved by the UBC Animal Care Committee.

Male WT, AKO and GzmB knockout mice were purchased from The Jackson Laboratory (Bar Harbor, ME, USA) and are all on a C57BL/6 background. DKO mice were generated by breeding GzmB knockout mice with AKO mice on site at the Genetic Engineered Models facility (James Hogg Research Centre, UBC/St. Paul's Hospital, Vancouver, BC, Canada). The mice used in this study were aged to either 7 weeks (young) or 37 weeks (old). Mice were fed *ad libitum* a regular chow diet (equal parts PicoLab Mouse Diet 20: 5058 (9% fat) and PicoLab Rodent Diet 20: 5053 (5% fat), LabDiet, Richmond, IN, USA) until 7 weeks of age. At 7 weeks, mice intended for the young groups underwent wounding surgery (described below). Mice intended for the old groups were either maintained on a regular chow diet or switched to a HFD (21.2% fat, TD.88137, Harlan Teklad; Madison, WI, USA) for 30 additional weeks, at which point they too underwent the wounding procedure. After healing for either 2, 8 or 16 days, mice were euthanized by isofluorane/carbon dioxide inhalation and tissue collected as described below.

Wound healing surgical procedure. Mice were given a full thickness skin wound on their mid backs. During surgery, mice were kept at a constant body temperature using a heating pad. Mice were initially anesthetized using isofluorane/oxygen mixture in an induction chamber. Once sedated, the mice were transferred from the chamber to a heating pad while their nose was placed in a nose cone providing the isofluorane/oxygen mixture to maintain anesthesia. Eye lube was applied to the eyes to prevent drying and back hair was shaved using an electric razor. After shaving, mice were given a subcutaneous injection of buprenorphine (0.05 mg/kg) away from the wound site for analgesia. The skin surface to be wounded was then sterilized using ethanol. A 1-cm diameter punch biopsy was then used to outline the wound area and the skin was then carefully excised using surgical scissors (including the panniculus carnosus muscle layer). Immediately following wounding, pictures were taken of the wound in the presence of a ruler to capture wound size at day 0. Mice were then allowed to recover and placed into individual cages during the healing phase of the study to prevent damage to the wound from other mice. Mice were allowed to heal for either 2, 8 or 16 days. At the selected time point, mice were euthanized by carbon dioxide inhalation and wounded tissue was harvested.

Tissue collection and processing. Following euthanasia, the wound was first cut in half vertically down the center. One half was then harvested and fixed in formalin for 24 h and embedded in paraffin for histological analysis and immunohistochemistry. The other half of the wound was flash frozen in liquid N_2 and stored at $-80\,^{\circ}C$ for analysis of ECM fragments by western blot.

Contraction, epidermal thickness and re-epithelialization measurements. Wound contraction was measured for all animals allowed to heal for 16 days. During the healing phase, the rate of contraction was measured every second day by taking digital pictures of the wounded area in the presence of a ruler. Contraction was then measured from the pictures using the imaging software, Image Pro Plus version 4.5.0.29 for Windows (Media Cybernetics Inc, Rockville, MD, USA). First, the outside of the wound at day 0 was traced and the original area of the wound was determined. All wound areas from subsequent days were normalized to the wound area from the corresponding animal at day 0 and expressed as a percent of the original wound size. Measurement of epidermal thickness was completed using hematoxylin and eosin (H&E)-stained sections at $\times 40$ magnification and were performed only on closed wounds. Wound edges featuring mature, unwounded collagen were identified and measurements were taken only within the boundary of the wound. Re-epithelialization was measured using H&E-stained skin cross-sections from mice at 2, 8 and 16 days of healing at $\times 40$ magnification. Beginning from the edge of the newly formed granulation tissue, re-epithelialization was measured as the distance along the basal keratinocyte layer that had migrated toward the center of the wound. For each section, two measurements were made, one on each end. For mice whose wounds were closed, the re-epithelialization distance was measured once and divided in half to represent the distance migrated from both ends of the wound.

Histology and immunohistochemistry. Paraffin-embedded skin cross-sections were stained with H&E for evaluation of morphology and with picrosirius red to examine collagen content. Collagen was observed in picrosirius red-stained sections using 100% polarized light and pictures were taken at a fixed exposure. GzmB, CD3 and F4/80 immunohistochemistry were performed by boiling deparaffinized slides in citrate buffer (pH 6.0) for 15 min. Background staining was blocked by incubating slides with 10% goat serum. The primary antibodies used were a rabbit anti-mouse GzmB antibody at a 1 : 100 dilution (Abcam, Cambridge, MA, USA), rabbit anti-mouse CD3 antibody at 1 : 800 dilution (Abcam) and rabbit anti-mouse F4/80 antibody at 1 : 50 dilution (Abcam). Slides were incubated with primary antibody at 4 °C overnight. Slides were then incubated with biotinylated goat anti-rabbit secondary antibody at a 1 : 350 dilution (Vector Laboratories, Burlingame, CA, USA) followed by ABC reagent (Vector Laboratories). Staining was visualized with DAB peroxidise substrate (Vector Laboratories). Decorin immunohistochemistry was performed by immersing deparaffinized slides in citrate buffer (pH 6.0) at 80 °C for 5 min. Slides were blocked with 10% rabbit serum and a goat anti-mouse decorin antibody (1 μg/ml; R&D Systems, Minneapolis, MN, USA) was used while slides incubated at 4 °C overnight. Biotinylated rabbit anti-goat secondary antibody was used (1 : 350) (Vector Laboratories) along with VECTASTAIN Elite ABC reagent (Vector Laboratories) and DAB substrate (Vector Laboratories) as described.

Histological quantification of collagen and decorin. Quantification of collagen was achieved by color segmentation in 5-μm thick fixed skin sections stained with picrosirius red. Images were taken at the wounded site under polarized light at $\times 20$ magnification. Using the imaging software, Image Pro Plus (version 4.5.0.29; Media Cybernetics Inc), the number of pixels within the area of interest whose intensity was above a set threshold was counted and expressed as the percent of total pixels. Decorin quantification of staining intensity was carried out using Aperio ImageScope (version 11.1.2.760; Aperio, Vista, CA, USA). The number of colored pixels within the designated area of interest was counted and expressed as the percent positive pixels. For consistency, both collagen and decorin quantification was measured within the wounded tissue to a depth of approximately 250 μm below the newly closed epidermal layer. Only wounds that had fully closed were used for these measurements.

Quantification of immune cells. Immune cell quantification was carried out using fixed skin cross-sections harvested at day 16 post-wounding. The area of the wound-containing granulation tissue was measured to a depth of 450 μm. Neutrophils and foam cells were counted at $\times 40$ magnification using slides stained with H&E and normalized to the area measured. T cells and macrophages were quantified using slides stained for CD3 and F4/80, respectively, as described above. Staining intensity was quantified using Aperio ImageScope. The number of color pixels (above a set threshold) identified were counted and expressed as the number of positive pixels per unit area.

Skin homogenization and analysis of ECM fragments. Frozen skin containing the wounded tissue was thawed and cut into identically sized 1 cm^2 pieces. Skin pieces were then placed into 1.5-ml tubes containing 350 μl CelLytic MT lysis buffer (Sigma-Aldrich, Oakville, ON, Canada), 4 μl protease inhibitor cocktail (Sigma-Aldrich) and a 7-mm stainless steel bead (Qiagen, Germantown, MD, USA). Tubes were then placed in a TissueLyser LT (Qiagen) and homogenized at 50 Hz for 4 min, three times for a total of 12 min. Tubes were placed on ice for 30 s in between the three homogenization cycles to prevent excessive heating. Tissue homogenate was then centrifuged at maximum r.p.m. at 4 °C and supernatant was collected. Total protein content was then measured in the supernatant solutions using a Nanodrop 8000 (Thermo Scientific, Waltham, MA, USA) and samples were then normalized by total protein before being used for western blotting experiments. Laemmli buffer (12 ml of 0.5 M Tris-HCl (pH 6.8), 8 ml glycerol, 2.4 g SDS, 1.86 g DTT and 50 mg bromophenol blue for a 20 ml 6 $\times$ stock solution) was then added to the supernatant samples followed by heating at 95 °C for 5 min. Samples were then run on a 6–15% gradient polyacrylamide gel and transferred to a nitrocellulose membrane. Membranes were blocked for 1 h using 2.5% skim milk followed by overnight incubation with rabbit anti-fibronectin antibody (Abcam) or sheep anti-vitronectin antibody (Affinity Biologicals Inc., Ancaster, Ontario, Canada) at a 1 : 1500 dilution in 2.5% skim milk. Membranes were then washed and incubated for 1 h with either IRDye 700-conjugated rabbit anti-sheep or IRDye 800-conjugated goat anti-rabbit secondary antibody at 1 : 10 000 (Rockland Inc., Gilbertsville, PA, USA). Following secondary antibody incubation, membranes were washed with PBS and detection of fibronectin and vitronectin was achieved using the Odyssey Infrared Imaging System (LI-COR Biotechnology, Lincoln, NE, USA).

Mouse ECM cleavage assay. Skin homogenate from a WT mouse wound harvested 8 days following wounding was generated using the

procedure described above. For this experiment, however, protease inhibitors were not included in the buffer in order to facilitate GzmB activity. A volume of 10 μl was then pipetted into microcentrifuge tubes. Mouse GzmB (Sigma-Aldrich) was added to a final concentration of either 0, 100, 200 or 400 nM. Tubes were then incubated at 37 °C for 24 h. Following the incubation, the reaction was stopped by adding Laemmli buffer (same recipe as above) and western blot analysis for fibronectin and vitronectin performed as described above.

Statistical analysis. The Kruskal–Wallis test with Dunn's Multiple Comparison post test or two-way ANOVA with Bonferroni post test was used for group comparison analyses and $P<0.05$ was considered significant. Statistical calculations were computed using GraphPad Prism version 5.01 for Windows, GraphPad Software (San Diego, California, USA, http://www.graphpad.com).

Conflict of Interest

David Granville is a Founder and Consultant to viDA Therapeutics, Inc. The remaining authors declare no conflict of interest.

Acknowledgements. This work was generously supported by a grant-in-aid from the Canadian Institutes of Health Research (DJG). PRH is supported by the CIHR Skin Research Training Centre and a Natural Sciences and Engineering Research Council of Canada Post Graduate Scholarship.

1. Sen CK, Gordillo GM, Roy S, Kirsner R, Lambert L, Hunt TK *et al.* Human skin wounds: a major and snowballing threat to public health and the economy. *Wound Repair Regen* 2009; **17**: 763–771.
2. Menke NB, Ward KR, Witten TM, Bonchev DG, Diegelmann RF. Impaired wound healing. *Clin Dermatol* 2007; **25**: 19–25.
3. Boivin WA, Cooper DM, Hiebert PR, Granville DJ. Intracellular versus extracellular granzyme B in immunity and disease: challenging the dogma. *Lab Invest* 2009; **89**: 1195–1220.
4. Cullen SP, Martin SJ. Mechanisms of granule-dependent killing. *Cell Death Differ* 2008; **15**: 251–262.
5. Waterhouse NJ, Clarke CJ, Sedelies KA, Teng MW, Trapani JA. Cytotoxic lymphocytes; instigators of dramatic target cell death. *Biochem Pharmacol* 2004; **68**: 1033–1040.
6. Lord SJ, Rajotte RV, Korbutt GS, Bleackley RC, Granzyme B. A natural born killer. *Immunol Rev* 2003; **193**: 31–38.
7. Afonina IS, Cullen SP, Martin SJ. Cytotoxic and non-cytotoxic roles of the CTL/NK protease granzyme B. *Immunol Rev* 2010; **235**: 105–116.
8. Froelich CJ, Pardo J, Simon MM. Granule-associated serine proteases: granzymes might not just be killer proteases. *Trends Immunol* 2009; **30**: 117–123.
9. Granville DJ. Granzymes in disease: bench to bedside. *Cell Death Differ* 2010; **17**: 565–566.
10. Hiebert PR, Granville DJ. Granzyme B in injury, inflammation, and repair. *Trends Mol Med* 2012; **18**: 732–741.
11. Zhang SH, Reddick RL, Piedrahita JA, Maeda N. Spontaneous hypercholesterolemia and arterial lesions in mice lacking apolipoprotein E. *Science* 1992; **258**: 468–471.
12. Plump AS, Smith JD, Hayek T, Aalto-Setala K, Walsh A, Verstuyft JG *et al.* Severe hypercholesterolemia and atherosclerosis in apolipoprotein E-deficient mice created by homologous recombination in ES cells. *Cell* 1992; **71**: 343–353.
13. Hui DY, Harmony JA, Innerarity TL, Mahley RW. Immunoregulatory plasma lipoproteins. Role of apoprotein E and apoprotein B. *J Biol Chem* 1980; **255**: 11775–11781.
14. Miyata M, Smith JD. Apolipoprotein E allele-specific antioxidant activity and effects on cytotoxicity by oxidative insults and beta-amyloid peptides. *Nat Genet* 1996; **14**: 55–61.
15. Pepe MG, Curtiss LK. Apolipoprotein E is a biologically active constituent of the normal immunoregulatory lipoprotein, LDL-In. *J Immunol* 1986; **136**: 3716–3723.
16. Zhang HL, Wu J, Zhu J. The immune-modulatory role of apolipoprotein E with emphasis on multiple sclerosis and experimental autoimmune encephalomyelitis. *Clin Dev Immunol* 2010; **2010**: 186813.
17. Hiebert PR, Boivin WA, Abraham T, Pazooki S, Zhao H, Granville DJ. Granzyme B contributes to extracellular matrix remodeling and skin aging in apolipoprotein E knockout mice. *Exp Gerontol* 2011; **46**: 489–499.
18. Feingold KR, Elias PM, Mao-Qiang M, Fartasch M, Zhang SH, Maeda N. Apolipoprotein E deficiency leads to cutaneous foam cell formation in mice. *J Invest Dermatol* 1995; **104**: 246–250.
19. Williams JZ, Barbul A. Nutrition and wound healing. *Surg Clin North Am* 2003; **83**: 571–596.
20. Sgonc R, Gruber J. Age-related aspects of cutaneous wound healing: a mini-review. *Gerontology* 2013; **59**: 159–164.
21. Singer AJ, Clark RA. Cutaneous wound healing. *N Engl J Med* 1999; **341**: 738–746.
22. Asaga H, Kikuchi S, Yoshizato K. Collagen gel contraction by fibroblasts requires cellular fibronectin but not plasma fibronectin. *Exp Cell Res* 1991; **193**: 167–174.
23. Corbett SA, Schwarzbauer JE. Requirements for alpha(5)beta(1) integrin-mediated retraction of fibronectin-fibrin matrices. *J Biol Chem* 1999; **274**: 20943–20948.
24. Valenick LV, Hsia HC, Schwarzbauer JE. Fibronectin fragmentation promotes alpha4beta1 integrin-mediated contraction of a fibrin-fibronectin provisional matrix. *Exp Cell Res* 2005; **309**: 48–55.
25. Sethi KK, Yannas IV, Mudera V, Eastwood M, McFarland C, Brown RA. Evidence for sequential utilization of fibronectin, vitronectin, and collagen during fibroblast-mediated collagen contraction. *Wound Repair Regen* 2002; **10**: 397–408.
26. Taliana L, Evans MD, Dimitrijevich SD, Steele JG. Vitronectin or fibronectin is required for corneal fibroblast-seeded collagen gel contraction. *Invest Ophthalmol Vis Sci* 2000; **41**: 103–109.
27. Buzza MS, Zamurs L, Sun J, Bird CH, Smith AI, Trapani JA *et al.* Extracellular matrix remodeling by human granzyme B via cleavage of vitronectin, fibronectin, and laminin. *J Biol Chem* 2005; **280**: 23549–23558.
28. Choy JC, Hung VH, Hunter AL, Cheung PK, Motyka B, Goping IS *et al.* Granzyme B induces smooth muscle cell apoptosis in the absence of perforin: involvement of extracellular matrix degradation. *Arterioscler Thromb Vasc Biol* 2004; **24**: 2245–2250.
29. Hendel A, Granville DJ. Granzyme B cleavage of fibronectin disrupts endothelial cell adhesion, migration and capillary tube formation. *Matrix Biol* 2012; **2**: 14–22.
30. Kaiserman D, Bird CH, Sun J, Matthews A, Ung K, Whisstock JC *et al.* The major human and mouse granzymes are structurally and functionally divergent. *J Cell Biol* 2006; **175**: 619–630.
31. Boivin WA, Shackleford M, Vanden Hoek A, Zhao H, Hackett TL, Knight DA *et al.* Granzyme B cleaves decorin, biglycan and soluble betaglycan, releasing active transforming growth factor-beta1. *PLoS One* 2012; **7**: e33163.
32. Froelich CJ, Zhang X, Turbov J, Hudig D, Winkler U, Hanna WL. Human granzyme B degrades aggrecan proteoglycan in matrix synthesized by chondrocytes. *J Immunol* 1993; **151**: 7161–7171.
33. Chamberlain CM, Ang LS, Boivin WA, Cooper DM, Williams SJ, Zhao H *et al.* Perforin-independent extracellular granzyme B activity contributes to abdominal aortic aneurysm. *Am J Pathol* 2010; **176**: 1038–1049.
34. Omoto Y, Yamanaka K, Tokime K, Kitano S, Kakeda M, Akeda T *et al.* Granzyme B is a novel interleukin-18 converting enzyme. *J Dermatol Sci* 2010; **59**: 129–135.
35. Afonina IS, Tynan GA, Logue SE, Cullen SP, Bots M, Luthi AU *et al.* Granzyme B-dependent proteolysis acts as a switch to enhance the proinflammatory activity of IL-1alpha. *Mol Cell* 2011; **44**: 265–278.
36. Choy JC. Granzymes and perforin in solid organ transplant rejection. *Cell Death Differ* 2010; **17**: 567–576.
37. Thomas HE, Trapani JA, Kay TW. The role of perforin and granzymes in diabetes. *Cell Death Differ* 2010; **17**: 577–585.
38. Cullen SP, Brunet M, Martin SJ. Granzymes in cancer and immunity. *Cell Death Differ* 2010; **17**: 616–623.
39. Darrah E, Rosen A. Granzyme B cleavage of autoantigens in autoimmunity. *Cell Death Differ* 2010; **17**: 624–632.
40. Hendel A, Hiebert PR, Boivin WA, Williams SJ, Granville DJ. Granzymes in age-related cardiovascular and pulmonary diseases. *Cell Death Differ* 2010; **17**: 596–606.
41. Kim WJ, Kim H, Suk K, Lee WH. Macrophages express granzyme B in the lesion areas of atherosclerosis and rheumatoid arthritis. *Immunol Lett* 2007; **111**: 57–65.
42. Choy JC, McDonald PC, Suarez AC, Hung VH, Wilson JE, McManus BM *et al.* Granzyme B in atherosclerosis and transplant vascular disease: association with cell death and atherosclerotic disease severity. *Mod Pathol* 2003; **16**: 460–470.
43. Jarvelainen H, Puolakkainen P, Pakkanen S, Brown EL, Hook M, Iozzo RV *et al.* A role for decorin in cutaneous wound healing and angiogenesis. *Wound Repair Regen* 2006; **14**: 443–452.
44. Dorshkind K, Montecino-Rodriguez E, Signer RA. The ageing immune system: is it ever too old to become young again? *Nat Rev Immunol* 2009; **9**: 57–62.
45. McElhaney JE. The unmet need in the elderly: designing new influenza vaccines for older adults. *Vaccine* 2005; **23**(Suppl 1): S10–S25.
46. Chandra RK. Nutrition and the immune system: an introduction. *Am J Clin Nutr* 1997; **66**: 460S–463S.
47. Yager DR, Nwomeh BC. The proteolytic environment of chronic wounds. *Wound Repair Regen* 1999; **7**: 433–441.
48. Danielson KG, Baribault H, Holmes DF, Graham H, Kadler KE, Iozzo RV. Targeted disruption of decorin leads to abnormal collagen fibril morphology and skin fragility. *J Cell Biol* 1997; **136**: 729–743.
49. Weber IT, Harrison RW, Iozzo RV. Model structure of decorin and implications for collagen fibrillogenesis. *J Biol Chem* 1996; **271**: 31767–31770.
50. Ang LS, Boivin WA, Williams SJ, Zhao H, Abraham T, Carmine-Simmen K *et al.* Serpina3n attenuates granzyme B-mediated decorin cleavage and rupture in a murine model of aortic aneurysm. *Cell Death Dis* 2011; **2**: e209.

51. Grinnell F, Ho CH, Wysocki A. Degradation of fibronectin and vitronectin in chronic wound fluid: analysis by cell blotting, immunoblotting, and cell adhesion assays. *J Invest Dermatol* 1992; **98**: 410–416.
52. Wysocki AB, Grinnell F. Fibronectin profiles in normal and chronic wound fluid. *Lab Invest* 1990; **63**: 825–831.
53. Stanley CM, Wang Y, Pal S, Klebe RJ, Harkless LB, Xu X *et al.* Fibronectin fragmentation is a feature of periodontal disease sites and diabetic foot and leg wounds and modifies cell behavior. *J Periodontol* 2008; **79**: 861–875.
54. Ongenae KC, Phillips TJ, Park HY. Level of fibronectin mRNA is markedly increased in human chronic wounds. *Dermatol Surg* 2000; **26**: 447–451.
55. Hynes RO. Integrins: bidirectional, allosteric signaling machines. *Cell* 2002; **110**: 673–687.
56. Ugarova TP, Ljubimov AV, Deng L, Plow EF. Proteolysis regulates exposure of the IIICS-1 adhesive sequence in plasma fibronectin. *Biochemistry* 1996; **35**: 10913–10921.
57. Poe M, Blake JT, Boulton DA, Gammon M, Sigal NH, Wu JK *et al.* Human cytotoxic lymphocyte granzyme B. Its purification from granules and the characterization of substrate and inhibitor specificity. *J Biol Chem* 1991; **266**: 98–103.
58. Murphy ME, Moult J, Bleackley RC, Gershenfeld H, Weissman IL, James MN. Comparative molecular model building of two serine proteinases from cytotoxic T lymphocytes. *Proteins* 1988; **4**: 190–204.

Supplementary Information accompanies this paper on Cell Death and Differentiation website (http://www.nature.com/cdd)